

<https://doi.org/10.1038/s42005-024-01756-w>

Validity of gyrokinetic theory in magnetized plasmas

Check for updates

Haotian Chen¹ , Liu Chen^{2,3}, Fulvio Zonca^{2,3}, Jiquan Li¹ & Min Xu¹

Gyrokinetics, as a reduced kinetic theory derived from adiabaticity, provides a general framework for the long-term dynamics of magnetized plasmas. While its validity limits are stated in terms of formal expansion parameters, more quantitative test of such is not widely mentioned even if it existed. Here we show, by detailed analyses of the Hamiltonian map with a test particle model, that gyrokinetic theory rests on the inherent nature of particle dynamics as a boundary layer problem. For low-frequency fluctuations, we demonstrate the existence of a frequency-independent threshold in the normalized amplitude, below which gyrokinetics is generally applicable. However, this threshold becomes sensitive to wave parameters in the high-frequency regime, which raises concerns about the generality of high-frequency gyrokinetic theory. Further analyses indicate that constructing a reduced kinetic equation based on superadiabaticity is not feasible. These findings contribute to a deeper understanding of the basic physics behind gyrokinetic theory.

Magnetized plasmas are ionized gases in which the ambient magnetic field significantly alters particle trajectories. They are known to play crucial roles in various fields, including fusion research, solar-terrestrial and astrophysical environments, and plasma-based industries. Physically, the fundamental challenge in understanding magnetized plasmas is the vast disparity between the very fast gyromotion time scale of a charged particle and the much slower characteristic time scales for collective instabilities. Gyrokinetics provides a unified framework for describing the long-term spatiotemporal evolution of magnetized plasmas (see refs. 1–3 and references therein). As one of the major achievements in modern plasma physics, this theory was established by an asymptotic construction of the magnetic moment adiabatic invariant $\bar{\mu}$, initially through the gyro-averaging method^{4–8} and later through the Lie-transform perturbation theory^{9–13}. The details of the charged particle's gyromotion are not of dynamical importance in the resulting gyrokinetic equation, which thereby reduces the kinetic problem from six dimensions to five. After half a century of intense pursuit, gyrokinetics now is the basis of numerous simulation codes and theoretical models used to study plasma instabilities, turbulence, and transport processes^{1,2,14–16}. A notable example in this regard is the recent launch of ambitious simulation projects that strive to deliver a high-fidelity whole-device model of magnetic fusion devices within the gyrokinetic framework (see, e.g., ref. 17).

Despite its practical success, the validity regime of gyrokinetic theory is typically stated by the nonlinear gyrokinetic ordering in terms of the formal expansion parameters^{1,8,18} and often assumed. The gyrokinetic theory is a reduced kinetic theory derived from adiabaticity. To ensure its generality, it

is essential to establish the robustness of adiabatic invariant across a wide range of plasma conditions. Previous studies, however, mainly focus on the construction of adiabatic invariant^{4,19–21}, a clear physics picture of the destruction mechanism is still lacking. The aim of this study is to illuminate what kind of physics sets the validity limits of gyrokinetic theory. Below, we will perform a thorough analysis of the nonlinear particle dynamics to investigate (i) under which conditions the adiabaticity would be broken and, accordingly the gyrokinetic theory would become invalid; (ii) why the high-frequency gyrokinetic theory, which was developed in the early 1980s^{18,22–26}, has not gained much popularity in implementation; (iii) whether the superadiabaticity²⁷ could also be utilized to construct a reduced kinetic theory.

In this work, we show the conventional ordering assumption is not precise enough for the strict validity of the gyrokinetic theory. The particle dynamics must constitute a boundary layer problem to guarantee the persistent existence of adiabatic invariant over a reasonably wide range of conditions. Consequently, in contrast to previous ordering arguments which are semi-quantitative in nature, we find a quantitative, frequency-independent threshold in the normalized amplitude below which the gyrokinetic theory is generally valid for low-frequency perturbations. Given the ordering of spatiotemporal scales and fluctuation strength in the standard low-frequency gyrokinetic theory¹, one could conclude that the corresponding normalized fluctuation level is considerably lower than the threshold. Therefore, the existence of such a threshold exhibits the robustness of the low-frequency gyrokinetic theory. The adiabaticity in high-frequency regimes, however, is sensitive to wave parameters, which

¹Southwestern Institute of Physics, Chengdu, 610041, China. ²Institute for Fusion Theory and Simulation and School of Physics, Zhejiang University, Hangzhou, 310027, China. ³Center for Nonlinear Plasma Science and C.R. ENEA Frascati-C.P. 65, Frascati, 00044, Italy. e-mail: chenhaotian@swip.ac.cn

raises concerns about the fundamental hypotheses of high-frequency gyrokinetic theory. Further analyses suggest that it is not possible to construct a reduced kinetic equation from superadiabaticity.

Results

The model

To elucidate the key physics involved in these highly complex problems, we restrict our attention to Taylor’s model⁴. This paradigm concerns the charged particle motion in a uniform magnetic field $\mathbf{B} = B\mathbf{e}_z$ with transverse perturbations, which, after a straightforward derivation, is described by the Hamiltonian

$$H = \frac{1}{2}(p^2 + q^2) + A \cos \omega t \cos q. \quad (1)$$

Here ω is the wave frequency and time is normalized to the gyroperiod $\Omega^{-1} = mc/eB$, with e being the charge and m the mass. Though simple, Taylor’s model is of fundamental importance in magnetized plasmas and was one of the seminal bases for the modern development of gyrokinetic theory¹. It represents the simplest paradigm for wave-particle dynamics in both the electrostatic drift wave (with $A = -k_{\perp}^2 e\delta\phi / (m\Omega^2)$)¹ and shear Alfvén wave (with $A = (k_{\perp} v_A / \Omega)(\delta B_{\perp} / B)$)²⁸ (see Methods, section ‘Derivation of the model Hamiltonian’), where k_{\perp} is the perpendicular wavenumber, v_A denotes the Alfvén velocity, and $\delta\phi$ and δB_{\perp} are, respectively, amplitudes of the fluctuating electrostatic potential and magnetic field. Note that here, the nonlinearity parameter A is determined by the spatial scale and amplitude of the perturbation, but is independent of the wave frequency. The particle dynamics in Eq. (1) can be conceptually separated into two parts: the gyromotion about the background magnetic field (the $q^2/2$ term), and the wave-particle trapping due to the perturbation (the $A \cos \omega t \cos q$ term). Furthermore, one can easily verify that the phase space flow arising from Eq. (1) exhibits time-reversal symmetry. Whenever $(q(t), p(t))$ is an orbit of the system with the initial condition (q_0, p_0) , both $(-q(-t), p(-t))$ and $(q(-t), -p(-t))$ will be physically allowable orbits, with the initial conditions $(-q_0, p_0)$ and $(q_0, -p_0)$, respectively. For periodic orbits, the associated dynamical invariant can be formulated as the action integral

$$I = \oint_{\gamma} p dq, \quad (2)$$

where γ is a closed orbit at constant time.

Further progress is possible if one introduces a variable h conjugate to t , yielding the extended phase space Hamiltonian

$$\mathcal{H} = \frac{1}{2}(p^2 + q^2) + A \cos \omega t \cos q - h. \quad (3)$$

In this way, the time-dependent one-dimensional Hamiltonian system is replaced by a two-dimensional Hamiltonian system where time plays a role analogous to that of an angle variable. Technically, to illustrate the long time scale ($\omega t \gg 1$) dynamical complexity of the system (which determines the existence of invariants), we construct the Poincaré map in extended phase space: $\mathbf{x}_{n+1} = \mathcal{M}_T \mathbf{x}_n$, where $\mathbf{x} = (q, p)$, and the mapping \mathcal{M}_T is defined such that the point \mathbf{x}_n at t_n is advanced by Eq. (3) to the next crossing point \mathbf{x}_{n+1} at $t_{n+1} = t_n + T$, with $T = 2\pi/\omega$.

Stability analysis

The global property of a Hamiltonian system can be understood by examining the orbits close to fixed points, which are either elliptic (stable) or hyperbolic (unstable). As depicted in Fig. 1, \mathcal{M}_T exhibits two different types of fixed points in accordance with the significance of nonlinearity. The primary fixed point $\mathbf{x}_p = (0, 0)$ is also the fixed point of the original system (1). It becomes unstable when the linear parametric resonance²⁹ occurs. Secondary fixed points \mathbf{x}_s , as assured by Poincaré–Birkhoff theorem³⁰, are

nonlinearly generated by a finite amplitude perturbation, half of which are elliptic and the other half hyperbolic in an alternating sequence. In general, the stability of secondary fixed points is not amenable to analytical analysis, numerical computations are mandatory.

To clarify the nature of the primary fixed point, linear stability analysis has been performed analytically via a perturbative treatment [Methods, section ‘Stability of primary fixed point’]. It follows that different unstable domains can be labeled by the marginal stability condition ($\omega = 2/m, A = 0$), with m a positive integer. Notably, a numerical evaluation of the linear growth rate $\text{Im}\lambda$ (see Fig. 2) identifies two distinct regimes. In the high-frequency regime with $\omega \gtrsim \mathcal{O}(10^{-1})$, the threshold amplitude A_c varies rapidly with ω . However, the low-frequency regime ($\omega \lesssim \mathcal{O}(10^{-1})$) is

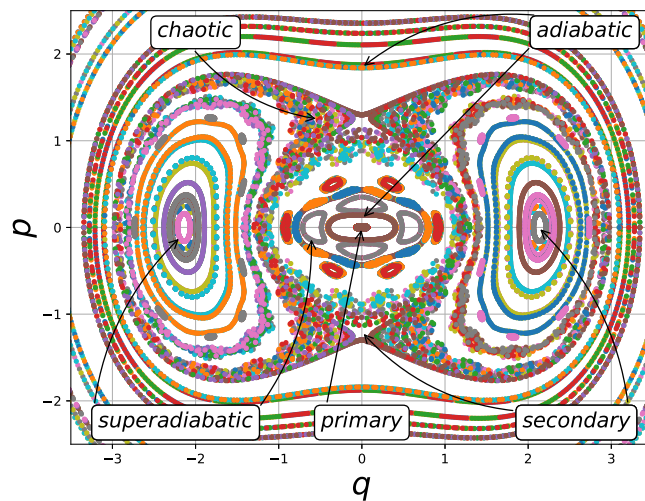


Fig. 1 | Examples of (primary and secondary) fixed points and (adiabatic, superadiabatic, and chaotic) orbits. Colors indicate distinct particles in the phase space, and $\mathbf{x} = (q, p)$ are the canonical coordinates. In this case, first, we evolve 180 particle orbits in time according to the Hamiltonian (1) for $\omega = 0.5$ and $A = 1.3$, with initial conditions (q_0, p_0) selected randomly in $[-5, 5] \times [-4, 4]$. Then the phase space portrait of the 2D Hamiltonian map $\mathbf{x}_{n+1} = \mathcal{M}_T \mathbf{x}_n$ is constructed such that the point \mathbf{x}_n at t_n is advanced to the next crossing point \mathbf{x}_{n+1} at $t_{n+1} = t_n + T$, with the wave period $T = 2\pi/\omega$.

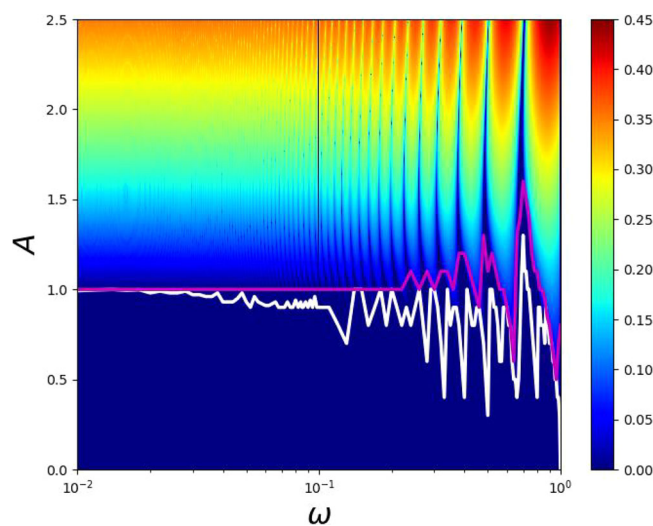


Fig. 2 | Stability diagram for the Taylor’s model. The color contours show $\text{Im}\lambda$ of Eq. (17), which measures the growth rate of separation of initially close orbits near the primary fixed point $\mathbf{x} = (0, 0)$. ω and A are the wave frequency and amplitude, respectively. The color bar represents the magnitude of $\text{Im}\lambda$. The white (magenta) line is the threshold numerically evaluated for the onset of superadiabatic (chaotic) orbits.

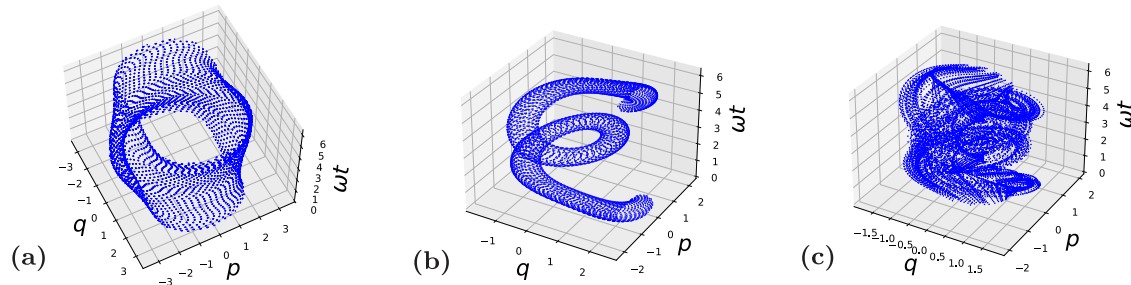


Fig. 3 | Comparison of the adiabatic, superadiabatic, and chaotic orbits in the extended phase space. The orbits are plotted for $A = 1.3$ and $\omega = 0.5$ with different initial conditions (q_0, p_0) : $(q_0 = 3.2, p_0 = 0)$ for the adiabatic orbit in (a), $(q_0 = 2.5, p_0 = 0)$ for the superadiabatic orbit in (b), and $(q_0 = 1.0, p_0 = 0)$ for the chaotic orbit in (c).

characterized by a dense spectrum corresponding to high-order resonances with $m \gg 1$, where $\text{Im}\lambda$ is insensitive to m and A_c piles up at a constant value $A_c = 1$.

The dynamical features of the system are intrinsically linked to the type of fixed points and, as illustrated in Fig. 1, can be put into three categories. The adiabatic orbit rotates with respect to the primary fixed point in the Poincaré map. The associated Kolmogorov–Arnold–Moser (KAM) torus³⁰ is deformed but remains intact topologically. It possesses the adiabatic invariant $\bar{\mu}$, which can be derived from Eq. (2) via a perturbative treatment, as in ref. 4. In regions of phase space where resonances take place, the original KAM torus will be destroyed, and the perturbation series for $\bar{\mu}$ fails to converge³⁰. Nonetheless, the emergence of a new KAM torus gives rise to a superadiabatic invariant²⁷, leading to the orbit rotating around a secondary fixed point. We refer to this type of orbit as the superadiabatic orbit. The distinguishing feature of chaotic orbits is the destruction of separating KAM tori. Quantitatively, the chaotic orbit in the present study is determined by the finite size Lyapunov exponent λ_L (for details, see “Methods: Lyapunov analysis of orbit topology”). Examples in Fig. 3 show the topological differences between adiabatic, superadiabatic, and chaotic orbits in extended phase space. The orbit in Fig. 3c displays a chaotic behavior with $\lambda_L \approx 0.014$.

We now examine the transition from adiabatic to superadiabatic/chaotic orbits by scanning A and ω . A result, shown by the white line in Fig. 2, is the identification of a quantitative, frequency-independent threshold $A_c \approx 1$ for $\omega \lesssim \mathcal{O}(10^{-1})$, which ensures the general applicability of adiabaticity in the low-frequency regime. To understand the physics of this threshold, we notice that Eq. (1) can be rendered into a boundary layer problem in the low-frequency limit, yielding

$$\omega^2 \frac{d^2 q}{d\theta^2} + q - A \cos \theta \sin q = 0, \quad (4)$$

with $\theta = \omega t$. Equation (4) displays manifestly the disparity between the short gyromotion time scale ($|\partial_\theta| \sim \omega^{-1}$), the wave-particle trapping time scale ($|\partial_\theta| \sim \sqrt{A}/\omega$), and the long time scale of the wave period ($|\partial_\theta| \sim 1$). On the gyromotion time scale, $\cos \theta$ can be treated as a constant, and one can easily show that the primary fixed point becomes unstable when $A > 1$, in agreement with Fig. 2. Here, the adiabaticity threshold $A_c = 1$ could be interpreted as the condition that the wave-particle trapping frequency ($\approx \sqrt{A}$) of resonant particles is comparable to the gyrofrequency ($=1$). On the long time scale $\partial_\theta \sim 1$, we have $q - A \cos \theta \sin q \approx 0$, then the secondary fixed points, which appear on time scales long compared to the wave period, are only possible if $A \approx |q/\sin q| \geq 1$. Additionally, numerical analyses suggest that $A_c = 1$ also gives a quantitative estimate for the chaotic threshold in low-frequency regime, as seen in Fig. 2. There are no superadiabatic or chaotic orbits for $A < 1$ in the low-frequency limit (see for example, Fig. 4a, b). Figure 4c shows that a chaotic layer arises as the homoclinic tangle³⁰ formed in the proximity of the hyperbolic primary fixed point. But the onset of chaos via the heteroclinic tangle³⁰, originating from unstable hyperbolic secondary fixed points, is observed as well (see Fig. 4d).

Validity of gyrokinetic theory

From the discussion above, it follows that the gyrokinetic theory is valid in the low-frequency regime. Even though this is consistent with the gyrokinetic ordering assumptions¹, the underlying physical interpretation is substantially different. The formal validity of gyrokinetic theory relies on the particle dynamics constituting a boundary layer problem in the present paradigm. This requirement establishes a quantitative, frequency-independent adiabaticity threshold, ensuring the persistent existence of the adiabatic invariant across a wide range of conditions. Thus, here, the validity of the gyrokinetic theory is a quantitative issue. Once below the threshold, gyrokinetics exhibits equal accuracy for all low-frequency waves. In the conventional qualitative paradigm, however, the low-frequency gyrokinetic theory is expected to be more accurate for the wave with lower frequency. Therefore, the inherent nature of particle dynamics as a boundary layer problem is essential for the validity of gyrokinetic theory. Specifically, recalling the spatiotemporal scales and relative fluctuation levels assumed in the low-frequency nonlinear gyrokinetic theory¹: $k_\perp v/\Omega \sim \mathcal{O}(1)$, $|\omega/\Omega| \ll 1$ and $|e\delta\phi/mv^2|, |\delta B_\perp/B| \ll 1$, one can readily show that the associated normalized fluctuation amplitude is typically lower than the threshold $A_c = 1$. The existence of such a quantitative and frequency-independent adiabaticity threshold thus reveals the robustness of the standard low-frequency gyrokinetic theory.

The separation of time scales does not apply for high-frequency perturbations. Accordingly, Fig. 2 shows that both the superadiabatic and chaotic thresholds are highly sensitive to the wave frequency. Thus the adiabaticity is not universally preserved, as opposed to the low-frequency case. This difference calls into question the validity of high-frequency gyrokinetic theory, which is derived from the assumption of adiabatic orbits^{18,24–26}. In addition, the breakdown of adiabaticity also vitiates the fundamental hypothesis of high-frequency gyrokinetics that the existence of gyrocenter coordinates is independent of ω . More specifically, noting that the perpendicular particle velocity in the present uniform plasma model satisfies $v_x \propto \rho$ and $v_y \propto q^4$, the phase space portraits of \mathcal{M}_T (shown in Fig. 5) indicate that the near identity transformation between the particle and gyrocenter coordinates, which is expressed as an asymptotic expansion in powers of the wave amplitude in Lie perturbation theory^{1,2,18,24}, will be invalidated by the presence of superadiabatic/chaotic orbits. The high-frequency gyrokinetic theory is, therefore, strictly valid only in the linear limit with $A = 0^{+22,23}$. Nevertheless, when considering small but finite amplitude perturbations, the linear high-frequency gyrokinetic theory becomes inadequate for describing the particle dynamics near resonant points ($\omega = 2/m$), due to the neglect of parametric resonance effect. Consequently, it cannot be utilized to develop quasilinear or weak turbulence theories.

Unlike in the low-frequency regime, Fig. 2 shows that while high-frequency perturbations break the adiabaticity more easily, the onset of chaos deviates significantly from the superadiabatic threshold. In this situation, one may attempt to construct a new reduced kinetic theory from the superadiabatic invariant. Unfortunately, this possibility is excluded. First, the intrinsically nonperturbative nature of superadiabatic orbits and

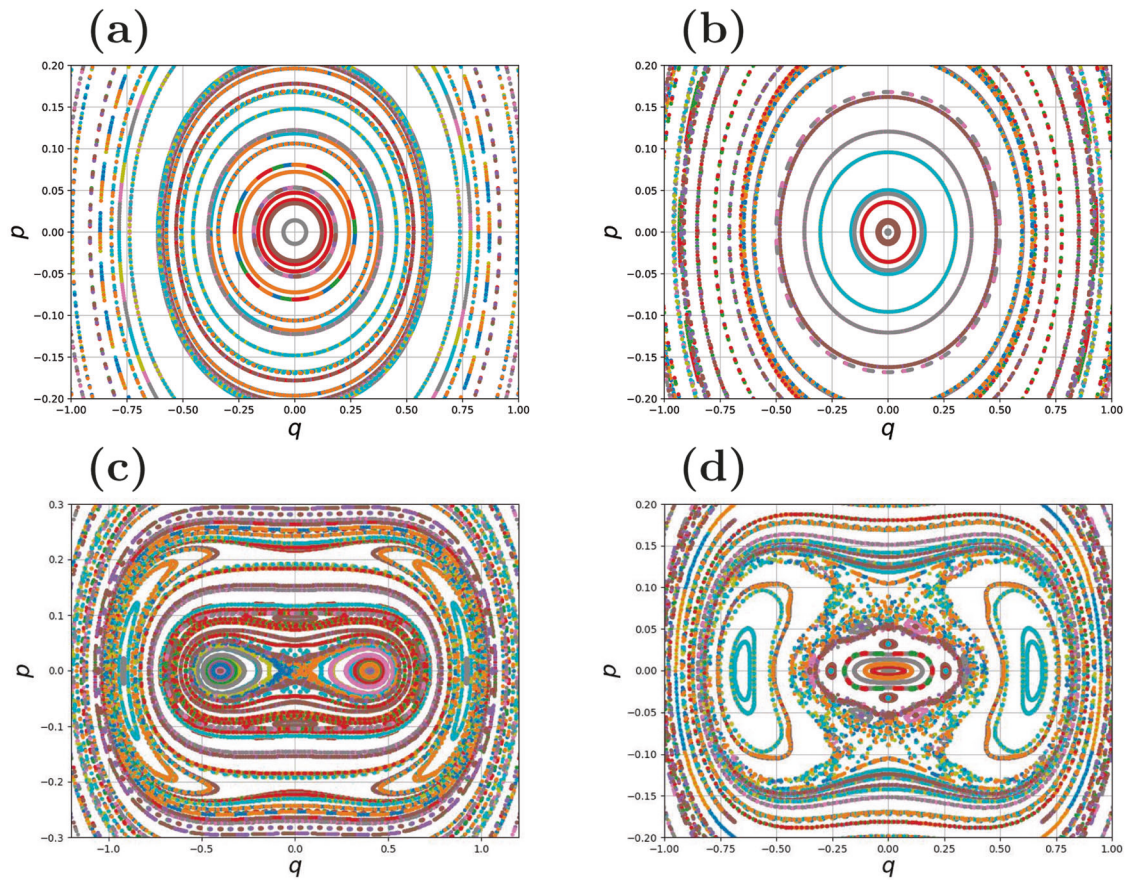


Fig. 4 | Phase space portrait of the 2D Hamiltonian map in low-frequency regime. Colors indicate distinct particles. In this case, we evolve 180 particle orbits in time according to the Hamiltonian (1) for **a** $\omega = 0.06$, $A = 0.9$, **b** $\omega = 0.059$, $A = 0.9$, **c** $\omega = 0.06$, $A = 1.01$, and **d** $\omega = 0.059$, $A = 1.01$, where initial conditions (q_0, p_0) are selected

randomly in $[-3, 3] \times [-1.5, 1.5]$. Then the 2D Hamiltonian map $\mathbf{x}_{n+1} = \mathcal{M}_T \mathbf{x}_n$ is constructed such that the point \mathbf{x}_n at t_n is advanced to the next crossing point \mathbf{x}_{n+1} at $t_{n+1} = t_n + T$, with the wave period $T = 2\pi/\omega$.

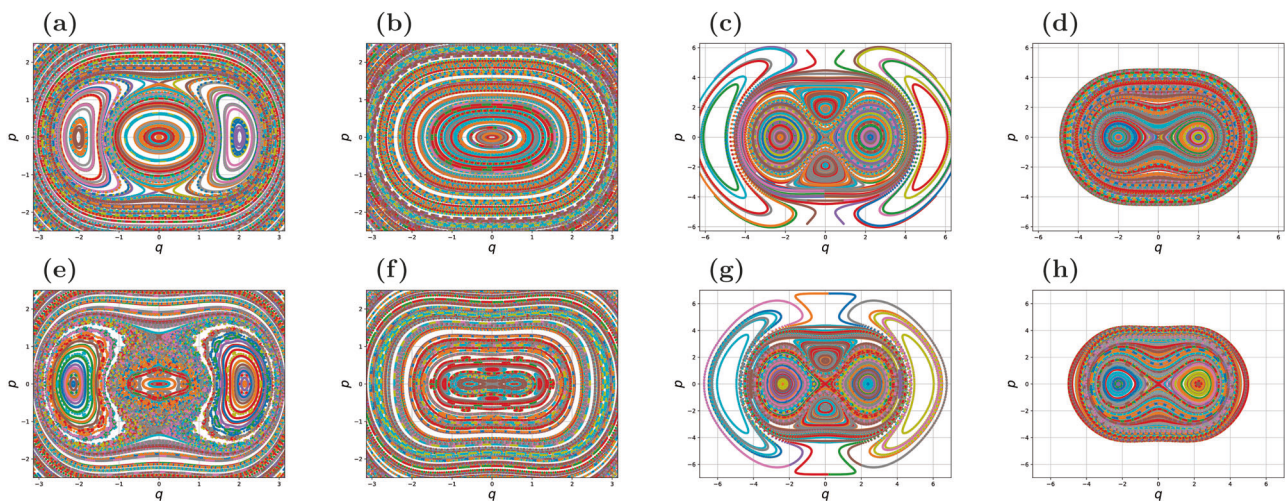


Fig. 5 | Phase space portrait of the 2D Hamiltonian map in a high-frequency regime. Colors indicate distinct particles. In this case, we evolve 180 particle orbits in time according to the Hamiltonian (1) for **a** $\omega = 0.50$, $A = 0.9$, **b** $\omega = 0.52$, $A = 0.9$, **c** $\omega = 1.00$, $A = 0.9$, **d** $\omega = 0.98$, $A = 0.9$, **e** $\omega = 0.50$, $A = 1.3$, **f** $\omega = 0.52$, $A = 1.3$,

g $\omega = 1.00$, $A = 1.3$, and **h** $\omega = 0.98$, $A = 1.3$, where initial conditions (q_0, p_0) are selected randomly in $[-5, 5] \times [-4, 4]$. Then the 2D Hamiltonian map $\mathbf{x}_{n+1} = \mathcal{M}_T \mathbf{x}_n$ is constructed such that the point \mathbf{x}_n at t_n is advanced to the next crossing point \mathbf{x}_{n+1} at $t_{n+1} = t_n + T$, with the wave period $T = 2\pi/\omega$.

the associated complexity of phase space structures (cf. Fig. 5) make it difficult, if not impossible, to derive a comprehensive analytic description for the superadiabatic invariant. Secondly, a general reduced kinetic theory requires that all particles possess the same invariant over a reasonably broad

range of conditions. However, Fig. 5 demonstrates that different particles could have distinct superadiabatic invariants at a fixed ω and, for each specific particle, the existence of corresponding superadiabatic invariant also depends sensitively on physical parameters.

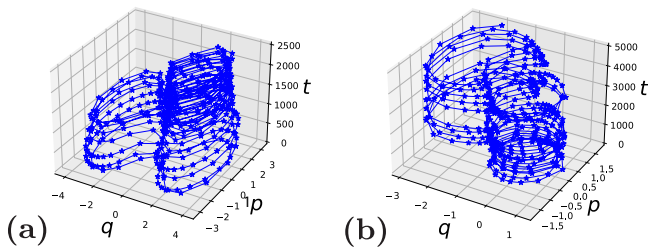


Fig. 6 | Typical evolution of the 2D Hamiltonian map for marginally chaotic orbits. The particle is randomly scattered into different types of orbits by homoclinic (a) or heteroclinic (b) tangles.

Whilst it is well established that the Lie series²⁰ of adiabatic/super-adiabatic invariant will not converge for chaotic orbits due to the presence of nonlinear resonance^{28,31}, intuition suggests that it might be possible to construct a gyrokinetic theory valid for a sufficiently long time via the gyro-averaging approach, if the orbit is only marginally chaotic. However, we find that once the chaotic threshold is exceeded, homoclinic and heteroclinic tangles can scatter the particle motion into different types of orbits without regularity, as shown in Fig. 6. In this scenario, the gyro-averaging (which refers to the integration along unperturbed adiabatic/superadiabatic orbits here) is ill-defined. It is thus impossible to properly account for the chaotic motion in both gyro-averaging and Lie perturbation approaches.

Discussion

We investigate the validity of gyrokinetic theory by employing the simplest paradigm. It is demonstrated that the conventional ordering assumption may not be precise enough for the strict validity of the gyrokinetic theory. The particle dynamics must constitute a boundary layer problem to guarantee the persistent existence of adiabatic invariance over a wide range of conditions. Accordingly, contrary to previous semi-quantitative ordering arguments, we find a quantitative, frequency-independent adiabaticity threshold A_c below which the gyrokinetic theory is universally valid in the low-frequency regime. In particular, using the spatiotemporal scales and fluctuation levels in the low-frequency nonlinear gyrokinetic theory, it can be estimated that the corresponding normalized fluctuation amplitude is considerably lower than the threshold A_c . In this sense, the existence of such a threshold reveals the robustness of the standard low-frequency gyrokinetic theory. In the high-frequency regime, however, the adiabaticity displays sensitive dependence on the wave parameters, which thereby raises concerns about the fundamental hypotheses of high-frequency gyrokinetic theory. Furthermore, unlike the situation with adiabaticity, it is not feasible to develop a new general reduced kinetic theory based on superadiabaticity.

From these considerations, we conclude that once the wave amplitude satisfies $A < A_c$, the gyrokinetic theory is reasonably applicable to the low-frequency drift-Alfvénic turbulence, whose wave frequency is typically $\mathcal{O}(10^{-2})$ smaller than the gyrofrequency¹⁶. Meanwhile, recalling the definition of A , it is worth mentioning the condition $A < A_c$ implies that the drift kinetic theory, which assumes $k_{\perp} \rightarrow 0^+$ and $\omega \ll \Omega$, applies for arbitrary fluctuation amplitudes, consistent with previous results^{32,33}. But still, it is of great concern whether one can employ the gyrokinetic theory, for example, in the vicinity of the separatrix of modern divertor tokamaks, where the radial wavenumber tends to diverge due to the magnetic topology change³⁴. Since there exist global nonlinear gyrokinetic codes including the divertor X-point region, such as XGC³⁵, it would be important to compare the predictions of turbulent fluxes and plasma profile evolution across the separatrix resulting from nonlinear gyrokinetic simulations with those of first-principle kinetic analyses at fixed boundary conditions (by this, we mean decoupling the well known complications of extending kinetic simulations into the plasma scrape-off layer.).

Moreover, we remark that while this study only deals with a single-frequency fluctuation in order to simplify the presentation, the present analysis can be readily generalized to turbulence with a broad spectrum, and the conclusions remain valid. In addition to the time scale considered here,

spatial variations may also break the adiabatic invariant, as observed numerically in spherical tokamaks^{36,37}. Though a similar approach could also apply here, a systematic and analytically treatable formalism incorporating both the spatial and time scales on an equal footing is beyond the intended scope of this study.

Methods

Derivation of the model Hamiltonian

Following⁴, we consider the motion of a charged particle immersed in a uniform magnetic field $\mathbf{B} = B\mathbf{e}_z$ with the electrostatic perturbation

$$\mathbf{E} = -\nabla\Phi \equiv \nabla[\delta\phi \cos(\omega t) \cos(k_{\perp}x)]. \quad (5)$$

The associated particle Hamiltonian can be written

$$H = \frac{1}{2m} [p_x^2 + (p_y - \frac{eBx}{c})^2 + p_z^2] + e\Phi, \quad (6)$$

where the momenta $p_y = mv_y + eBx/c$ and p_z are constant. Then, the equations of motion are

$$\begin{aligned} \dot{p}_x &= \frac{eB}{mc} (p_y - \frac{eBx}{c}) - ek_{\perp} \delta\phi \cos(\omega t) \sin(k_{\perp}x), \\ \dot{x} &= \frac{p_x}{m}. \end{aligned} \quad (7)$$

By taking $p_y = 0$, Eq. (7) becomes an oscillator under the influence of external force

$$\ddot{x} + \Omega^2 x = -\frac{ek_{\perp} \delta\phi}{m} \cos(\omega t) \sin(k_{\perp}x). \quad (8)$$

Normalizing the space to k_{\perp}^{-1} and time to Ω^{-1} , Eq. (8) is readily cast as

$$\ddot{q} + q = A \cos \omega t \sin q, \quad (9)$$

which is derivable from the Hamiltonian (1) with $A = -k_{\perp}^2 e\delta\phi / (m\Omega^2)$, $q = k_{\perp}x$, and $p = \dot{q}$. Therefore, it can be recognized that parameter A is the normalized amplitude of the perturbed force and quantifies the strength of nonlinearity.

Equation (1) offers a simple paradigm for the wave-particle dynamics in shear Alfvén wave (SAW)²⁸ as well. To see this, let us consider an obliquely propagating ($\mathbf{k} = k_z\mathbf{e}_z + k_x\mathbf{e}_x$) shear Alfvén wave, whose electromagnetic fluctuation, by employing the Walén relation³⁸, can be expressed as $\delta\mathbf{B} = \delta B_y\mathbf{e}_y$ and $\delta E = (v_A/c)\delta B_y\mathbf{e}_x$. Then the Lorentz equations of motion are

$$\begin{aligned} m\dot{v}_x &= \frac{e}{c} [v_y B + (v_A - v_z)\delta B_y], \\ v_y &= -\Omega x, \\ m\dot{v}_z &= \frac{e}{c} v_x \delta B_y, \end{aligned} \quad (10)$$

and the energy $v^2 = v_x^2 + v_y^2 + (v_z - v_A)^2$ is a constant of motion.

Although Eq. (10) states that SAW can influence the parallel particle dynamics and bring relevant extra-dimensions to the system, it was shown³⁹ that the particle motion is non-chaotic for parallel propagation SAWs ($\mathbf{k} = k_z\mathbf{e}_z$). The perpendicular dynamics with a finite k_x is essential for the chaotic behavior of the system⁴⁰. To provide analytical insights and, thus, clarity in illustration, we focus on the particles initially cold in the laboratory frame ($v_z^2(0) \ll v_A^2$). To the first order in $\delta B_y/B$, one arrives at the formula

$$\ddot{x} + \Omega^2 x = (v_A - v_z(0))\Omega \frac{\delta B_y}{B}. \quad (11)$$

Again, if we normalize x to k_{\perp}^{-1} and time to Ω^{-1} , and take the SAW frequency $\omega_A \simeq k_{\parallel} v_A / \Omega$, Eq. (11) can be rendered into

$$\ddot{q} + q = \frac{k_{\perp}(v_A - v_z(0))\delta B_y}{\Omega B}. \tag{12}$$

Writing $\delta B_y = \delta B_{\perp} \cos((\omega_A - k_{\parallel} v_z)t) \sin(k_{\perp} x)$ and $\omega = \omega_A - k_{\parallel} v_z(0) \simeq \omega_A$, Eq. (12) becomes identical to Eq. (9) with $A = (k_{\perp} v_A / \Omega)(\delta B_{\perp} / B)$ and $q = k_{\perp} x$.

Furthermore, it should be stressed that the arguments presented in the current study can also be applied to ascertain the existence of adiabaticity when retaining parallel dynamics. In particular, using $(v_z - v_A)^2 = v^2 - v_x^2 - v_y^2$, Eq. (12) can be cast as

$$\ddot{q} + q = \frac{\sigma \sqrt{k_{\perp}^2 v^2 - \Omega^2(q^2 + q'^2)} \delta B_{\perp}}{\Omega B} \cos(k_{\parallel} \int^t \sigma \sqrt{v^2 - \frac{\Omega^2}{k_{\perp}^2}(q^2 + q'^2)} \frac{dt'}{\Omega}) \sin q, \tag{13}$$

in which σ denotes the sign of $v_A - v_z$. For the primary fixed point, linearizing Eq. (13) around $(q = 0, p = 0)$ yields the same expression as Eq. (15) with $v^2 = (v_z(0) - v_A)^2$. Hence, Fig. 2 also characterizes the primary fixed point stability of the system (10). On the other hand, noting that Eq. (13) is a boundary layer problem in the low-frequency limit, we find the secondary fixed points appearing on long time scales are only possible if

$$\frac{k_{\perp} v \delta B_{\perp}}{\Omega B} \simeq \left| \frac{q}{\sqrt{1 - \frac{\Omega^2}{k_{\perp}^2 v^2}(q^2 + q'^2)} \cos(k_{\parallel} \int^t \sigma \sqrt{v^2 - \frac{\Omega^2}{k_{\perp}^2}(q^2 + q'^2)} \frac{dt'}{\Omega}) \sin q} \right| > 1. \tag{14}$$

As a result, the system (10) still possesses the quantitative and frequency-independent adiabaticity threshold $A_c = (k_{\perp} v / \Omega)(\delta B_{\perp} / B) = 1$ in the low-frequency regime.

Stability of primary fixed point

The derivation of the stability condition of the primary fixed point starts from the Hamiltonian in Eq. (1). By approximating $\cos q \simeq 1 - q^2/2$, the corresponding equation of motion reduces to a Mathieu equation:

$$\ddot{q} + (1 - A \cos \omega t)q = 0. \tag{15}$$

According to the Floquet theory, the formal solution of Eq. (15) can be expressed as

$$q = e^{i\lambda t} \sum_n Q_n e^{in\omega t}, \tag{16}$$

where the Floquet characteristic exponent λ is a measure of the rate of separation of orbits close to the primary fixed point. x_p is elliptic (hyperbolic) if λ is real (complex). Substituting Eq. (16) into Eq. (15) and following the procedure in ref. 41, one obtains

$$\lambda = \begin{cases} \frac{\omega}{\pi} \arcsin \sqrt{D(0) \sin^2(\frac{\pi}{\omega})}, & \omega \neq \frac{1}{2}, \\ \frac{\omega}{2\pi} \arccos[2D(\frac{\omega}{2}) - 1], & \omega = \frac{1}{2}, \end{cases} \tag{17}$$

where D is the determinant of an infinite tridiagonal matrix $\mathbf{D} = (d_{jk})$ with

$$d_{jk} = \begin{cases} 1 & \text{if } k = j, \\ \frac{A}{2|(\lambda + j\omega)^2 - 1|} & \text{if } k = j \pm 1, \\ 0 & \text{otherwise.} \end{cases} \tag{18}$$

l, j, k are integers. For sufficiently small $A \ll \omega^2/2$, an analytic expression for $D(0)$ can be concisely given as $D(0) \simeq 1 - RA^2$ with

$R \equiv (\pi/\omega) \cot(\pi/\omega)/2(4 - \omega^2)^{41}$. By means of Eq. (17), one can derive the threshold for hyperbolic x_p

$$A_c^2 = \begin{cases} R^{-1} & \text{if } R > 0, \\ R^{-1}(1 - \sin^{-2} \frac{\pi}{\omega}) & \text{otherwise.} \end{cases} \tag{19}$$

Equation (19) allows one to label different unstable domains using the marginal stability condition ($\omega = 2/m, A = 0$), with m a positive integer.

Lyapunov analysis of orbit topology

Chaotic orbits in this work are determined in terms of a modified version of the finite size Lyapunov exponent (FSLE) λ_L .

Consider at $t = 0$ a reference trajectory $x(0)$ and a perturbed trajectory $x'(0) = x(0) + \delta x(0)$, the basic idea behind FSLE is to quantify the average rate of error growth at different scales when subject to non-infinitesimal perturbations⁴². Specifically, let us first take an infinitesimal initial perturbation $\delta_{min} \ll 1$ and choose a set of thresholds at different scales $\delta_n = \delta_0 \rho^n$. Here, $\delta_{min} \ll \delta_0 \ll 1, n = 0, \dots, N, \rho > 1$, and δ_N accounts for the maximum allowed separation. The parameters we have adopted for the current study are $\delta_{min} = 10^{-6}, d_0 = |\delta x(0)| + 10^{-5}$ and $\rho = \sqrt{2}$. The trajectories are advanced using a fourth-order Runge–Kutta algorithm. After the perturbation has grown from δ_{min} to δ_0 , we measure the time $t_i(\delta_n)$ from δ_n to δ_{n+1} . A single error-doubling experiment completes when the error reaches δ_N . Then this procedure is repeated M times to obtain the set of doubling times $\{t_i(\delta_n)\}$ for $i = 1, \dots, M$ error-doubling experiments. The growth rate γ_i is estimated through the average of τ_i across different scales,

$$\gamma_i = \frac{\ln \rho}{\langle \tau_i(\delta_n) \rangle_{\delta}}. \tag{20}$$

We define the averaged FSLE as the averaging over doubling experiments $\lambda_L = \langle \gamma_i \rangle_M$. Numerically, we find Eq. (20) converges much faster than the FSLE originally given in ref. 42.

Data availability

The data depicted in the plots of this paper is available from the corresponding author upon reasonable request.

Received: 20 February 2024; Accepted: 24 July 2024;
Published online: 03 August 2024

References

1. Brizard, A. & Hahm, T. S. Foundations of nonlinear gyrokinetic theory. *Rev. Mod. Phys.* **79**, 421 (2007).
2. Krommes, J. A. The Gyrokinetic description of microturbulence in magnetized plasmas. *Annu. Rev. Fluid. Mech.* **44**, 175 (2012).
3. Catto, P. Practical gyrokinetics. *J. Plasma Phys.* **85**, 925850301 (2019).
4. Taylor, J. B. Magnetic moment under short wave electrostatic perturbations. *Phys. Fluids* **10**, 1357 (1967).
5. Rutherford, P. H. & Frieman, E. A. Drift instabilities in general magnetic field configurations. *Phys. Fluids* **11**, 569 (1968).
6. Taylor, J. B. & Hastie, R. J. Stability of general plasma equilibria - I formal theory. *Plasma Phys.* **10**, 479 (1968).
7. Catto, P. J. Linearized gyro-kinetics. *Plasma Phys.* **20**, 719 (1978).
8. Frieman, E. A. & Chen, L. Nonlinear gyrokinetic equations for low-frequency electromagnetic waves in general plasma equilibria. *Phys. Fluids* **23**, 302 (1982).
9. Littlejohn, R. G. A guiding center Hamiltonian: a new approach. *J. Math. Phys.* **20**, 2445 (1979).
10. Dubin, D. H. E. et al. Nonlinear gyrokinetic equations. *Phys. Fluids* **26**, 3524 (1983).
11. Hahm, T. S. et al. Nonlinear gyrokinetic theory for finite-beta plasmas. *Phys. Fluids* **31**, 1940 (1988).

12. Brizard, A. Nonlinear gyrokinetic Maxwell-Vlasov equations using magnetic co-ordinates. *J. Plasma Phys.* **41**, 541 (1989).
13. Sugama, H. Gyrokinetic field theory. *Phys. Plasmas* **7**, 466 (2000).
14. Horton, W. Drift waves and transport. *Rev. Mod. Phys.* **71**, 735 (1999).
15. Kikuchi, M. & Azumi, M. Steady-state tokamak research: core physics. *Rev. Mod. Phys.* **84**, 1807 (2012).
16. Chen, L. & Zonca, F. Physics of Alfvén waves and energetic particles in burning plasmas. *Rev. Mod. Phys.* **88**, 015008 (2016).
17. Bhattacharjee, A. & Wells, J. Preface to special topic: building the bridge to the exascale-applications and opportunities for plasma physics. *Phys. Plasmas* **28**, 090401 (2021).
18. Qin, H. Gyrokinetic perpendicular dynamics. *Phys. Plasmas* **6**, 1575 (1999).
19. Kruskal, M. Asymptotic theory of Hamiltonian and other systems with all solutions nearly periodic. *J. Math. Phys.* **3**, 806 (1962).
20. Dubin, D. H. E. & Krommes, J. A. *Stochasticity, Superadiabaticity, and the Theory of Adiabatic Invariants and Guiding-Center Motion. Long Time Prediction in Dynamics* (Wiley, 1992).
21. Qin, H. & Davidson, R. C. An exact magnetic-moment invariant of charged-particle gyromotion. *Phys. Rev. Lett.* **96**, 085003 (2006).
22. Chen, L. & Tsai, S. T. Electrostatic waves in general magnetic field configurations. *Plasma Phys.* **26**, 141 (1983).
23. Tsai, S. T., Van Dam, J. W. & Chen, L. Linear relativistic gyrokinetic equation in general magnetically confined plasmas. *Plasma Phys. Control. Fusion* **26**, 907 (1984).
24. Qin, H., Tang, W. M. & Lee, W. W. Gyrocenter-gauge kinetic theory. *Phys. Plasmas* **7**, 4433 (2000).
25. Kolesnikov, R. A. et al. High frequency gyrokinetic particle simulation. *Phys. Plasmas* **14**, 072506 (2007).
26. Yu, Z. & Qin, H. Gyrocenter-gauge kinetic algorithm for high frequency waves in magnetized plasmas. *Phys. Plasmas* **16**, 032507 (2009).
27. Rosenbluth, M. N. Superadiabaticity in mirror machines. *Phys. Rev. Lett.* **29**, 408 (1972).
28. Chen, L., Lin, Z. & White, R. On resonant heating below the cyclotron frequency. *Phys. Plasmas* **8**, 4713 (2001).
29. Arnold, V. I. *Mathematical Methods of Classical Mechanics* (Springer, 1989).
30. Lichtenberg, A. J. & Leiberman, M. A. *Regular and Chaotic Dynamics*. 2nd edn (Springer, 2010).
31. Jaeger, E. F. & Lichtenberg, A. J. Resonant modification and destruction of adiabatic invariants. *Ann. Phys.* **71**, 319 (1972).
32. Hazeltine, R. D. Recursive derivation of drift-kinetic equation. *Plasma Phys.* **15**, 77 (1973).
33. Chen, L., Zonca, F. & Chen, H. Unexpanded nonlinear electromagnetic gyrokinetic equations for magnetized plasmas. *Plasma Sci. Technol.* **22**, 102001 (2020).
34. Kadomtsev, B. B. *Tokamak Plasma: A Complex Physical System* (Institute of Physics Publishing, 1992).
35. Chang, C. S. et al. Gyrokinetic projection of the divertor heat-flux width from present tokamaks to ITER. *Nucl. Fusion* **57**, 116023 (2017).
36. Carlsson, J. Breakdown of adiabatic invariance in spherical tokamaks. *Phys. Plasma* **8**, 4725 (2001).
37. Escande, D. F. & Sattin, F. Breakdown of adiabatic invariance of fast ions in spherical tokamaks. *Nucl. Fusion* **61**, 106025 (2021).
38. Walén, C. On the theory of sunspots. *Ark. Mat. Astron. Fys* **30A**, 1, (1944).
39. Wu, C. S., Yoon, P. H. & Chao, J. K. Motion of ions influenced by enhanced Alfvén waves. *Phys. Plasma* **4**, 856 (1997).
40. Lin, Y. & Lee, L. C. Structure of reconnection layers in the magnetosphere. *Space Sci. Rev.* **65**, 59 (1993).
41. McLachlan, N. W. *Theory and Application of Mathieu Functions* (Clarendon Press, 1951).
42. Aurell, E. et al. Growth of non-infinitesimal perturbations in turbulence. *Phys. Rev. Lett.* **77**, 1262 (1996).

Acknowledgements

H.C. wishes to thank Y.R. Lin-Liu and R.L. Miller for their proposal and help in the initial phase of this work. The authors thank D.F. Escande and F. Sattin for stimulating discussions. This work was supported by the National Natural Science Foundation of China under Grant Nos. 12375213 and 12275071, and by the Innovation Program of Southwestern Institute of Physics (202301XWCX001). This work was also supported by the Italian Ministry for Foreign Affairs and International Cooperation Project under Grant No. CN23GR02.

Author contributions

H.C. designed the research and performed the analyses. L.C., F.Z., J.L., and M.X. contributed to the physical interpretation. H.C. wrote the manuscript, with feedback from all coauthors.

Competing interests

The authors declare no competing interests.

Additional information

Correspondence and requests for materials should be addressed to Haotian Chen.

Peer review information *Communications Physics* thanks Alain Brizard and the other, anonymous, reviewer(s) for their contribution to the peer review of this work.

Reprints and permissions information is available at <http://www.nature.com/reprints>

Publisher's note Springer Nature remains neutral with regard to jurisdictional claims in published maps and institutional affiliations.

Open Access This article is licensed under a Creative Commons Attribution-NonCommercial-NoDerivatives 4.0 International License, which permits any non-commercial use, sharing, distribution and reproduction in any medium or format, as long as you give appropriate credit to the original author(s) and the source, provide a link to the Creative Commons licence, and indicate if you modified the licensed material. You do not have permission under this licence to share adapted material derived from this article or parts of it. The images or other third party material in this article are included in the article's Creative Commons licence, unless indicated otherwise in a credit line to the material. If material is not included in the article's Creative Commons licence and your intended use is not permitted by statutory regulation or exceeds the permitted use, you will need to obtain permission directly from the copyright holder. To view a copy of this licence, visit <http://creativecommons.org/licenses/by-nc-nd/4.0/>.

© The Author(s) 2024, corrected publication 2024